Deep Learning Optimization for High-Power Laser Aberration Correction

Fernandes, G.G.D.[1,2]; Alexandrino, D.[1,2]; Silva, E.[1,2]; Matias, J.[1,2]; Pereira, J.[1,2]

[1]Instituto Superior Técnico

[2]Instituto de Plasmas e Fusão Nuclear

Abstract

High harmonic generation (HHG) is a nonlinear process that enables table-top generation of tunable, high-energy, coherent, ultrashort radiation pulses in the extreme ultraviolet (EUV) to soft X-ray range. These pulses find applications in photoemission spectroscopy in condensed matter physics [1], pump-probe spectroscopy for high-energy-density plasmas, and attosecond science. However, optical aberrations in the high-power laser systems required for HHG degrade beam quality and reduce efficiency. We present a machine learning approach to optimise aberration correction using a spatial light modulator (SLM). We implemented and compared Bayesian optimisation and convolutional neural network (CNN) methods to predict optimal Zernike polynomial coefficients for wavefront correction. Our CNN achieved promising results with 80.39% accuracy on test data, demonstrating the potential for automated aberration correction in HHG systems.

1   Introduction

High harmonic generation (HHG) is a nonlinear process in which the interaction between a high-intensity laser pulse and a material generates high-order harmonics (typically above the fifth harmonic) of the fundamental laser frequency, producing pulses with frequencies that are integer multiples of the initial pulse frequency.

The process can be understood using the **three-step model** [2]: (1) an electron tunnels out from the atomic potential, which is distorted by the intense laser field; (2) the freed electron is acceler- ated away from the atom by the driving field; (3) after half a laser period, the electric field reverses direction and acceler- ates the electron back toward the atomic potential, where it recombines and emits a high-energy photon. The nonlinear nature of this process typically results in pulse durations shorter than the initial driving pulse, enabling applications in **attosecond physics**, where extremely high temporal resolution is required.

1

2 Motivation

HHG requires a high-power laser that must be manipulated and focused to a small spot where the target gas is located. The optical apparatus used for this purpose introduces aberrations that degrade the beam quality and reduce the efficiency of HHG. These aberrations can be modelled using Zernike polynomials [3], where each polynomial order corresponds to a specific type of aberration, and the coefficients determine its magnitude and shape. Zernike polynomials provide a complete orthogonal basis for representing wavefront aberrations and are widely used in adaptive optics.

To correct these aberrations, we employ a **spatial light modulator (SLM)** as a controllable wavefront correction device. The SLM functions as a programmable diffractive element, composed of 1000×1000 pixels, where each pixel's refractive index can be controlled via an applied voltage. By appropriately configuring the voltage pattern across the SLM, it can effectively flatten an aberrated wavefront, compensating for optical distortions introduced by the system.

The core objective of this work is the development, testing, and implementation of machine learning methods to optimise the SLM voltage patterns for optimal laser focusing, thereby maximising HHG efficiency.

3 Experimental Apparatus

An initial simplified setup was used for developing and testing the optimisation algorithms. This setup comprised lenses, mirrors, the SLM, a laser, and a camera. The laser beam passed through several lenses to introduce controlled aberrations, then through the SLM for correction, and was finally focused onto a camera for characterisation.

The main experimental setup was the existing HHG system, into which the SLM was integrated. A high-power infrared pulsed laser was directed into a vacuum chamber, where it was focused onto a gas cell to generate high-order harmonics. At the end of the vacuum chamber, a Greateyes UV camera was used for detection and visualisation of the harmonics, providing data for the machine learning algorithms. The optical system was composed of several lenses, mirrors, other optical components, and, of course, the SLM. Of note are the attenuator that allowed control of the laser intensity; several irises that allowed for alignment and also some degree of control over the intensity, as well as a selection of the correct order beam[1]; a beam splitter that would split the laser onto an adjacent path into a Thorlabs camera that would gather data for an early form of the optimization algorithms that did not use data from the Greateyes UV camera yet. A diagram of the setup can be seen below, 1.

Initial integration of the SLM into the HHG system involved manual optimisation using data from the Thorlabs camera, with direct adjustment of aberration coefficients in the SLM settings.

After HHG was established, the oblique astigmatism coefficient in the SLM was swept from 0.03 to 0.24 in increments of 0.03. The data collected from the Greateyes camera were analysed to

---

[1]The diffraction grating like behavior of the SLM causes it to have multiple orders of diffracted beams, (zeroth-order not being diffracted by the SLM at all, etc.) we had then to make sure we only had the first-order diffracted beam going into the vacuum chamber, blocking the rest with an iris.
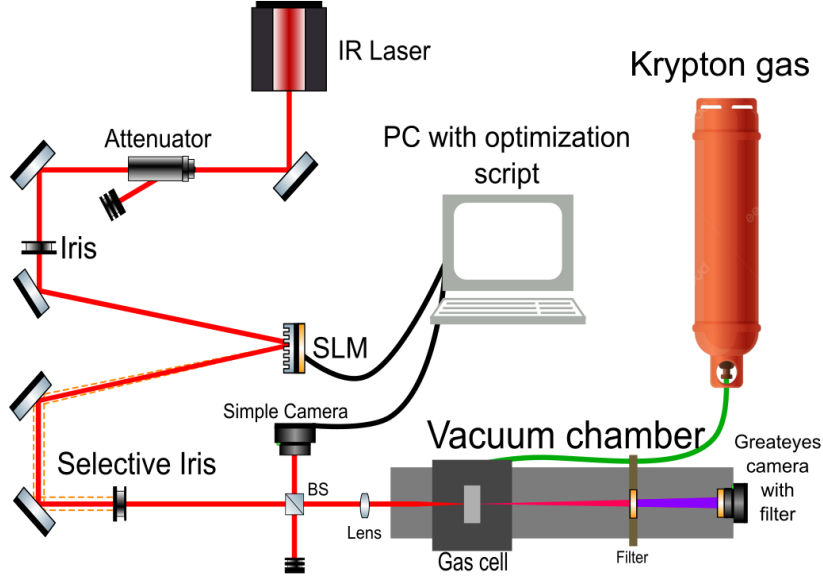
Figure 1: Final setup for HHG with SLM. The gas cell contains krypton. Filters remove all wavelengths from the beam post-HHG (represented in pink), except those corresponding to high-order harmonics in the XUV range (represented in purple). The dashed orange lines represent unwanted diffracted orders from the SLM, which are blocked by an iris.

produce the results shown in Figure 2.

As shown in Figure 2, it is possible to manually identify coefficients that significantly affect the total signal. However, for higher-dimensional optimisation problems (with many parameters beyond oblique astigmatism), this manual approach becomes impractical. To accelerate this process, we implemented machine learning approaches, detailed in Sections 4 and 6.

4 Bayesian Optimization

4.1 The bayesopt Function

MATLAB's `bayesopt` function implements Bayesian optimisation, a method for finding optimal hyperparameters by building a probabilistic model of the objective function. The function `bayesopt(fun,vars)` attempts to find values of `vars` that minimise `fun(vars)`. Although designed for minimisation, it can be used for maximisation by negating

the objective function.

4.2 Optimizing The Peak Intensity

We adapted a previously developed script to use Bayesian optimisation for optimising the performance of a system comprising a camera, an SLM, and Zernike polynomial-based holographic correction. The objective was to optimise focal spot quality by adjusting the amplitudes of different Zernike modes. Specifically, we optimised five Zernike modes: focus, vertical astigmatism, oblique astigmatism, vertical coma, and horizontal coma.

The code first initialises the Thorlabs TLCamera, configuring gain and exposure time. The camera's bit depth is used to determine the maximum pixel value (`maxPixelValue`).

The Bayesian optimisation process is iterative. To optimise the focus mode, we define an objective func-
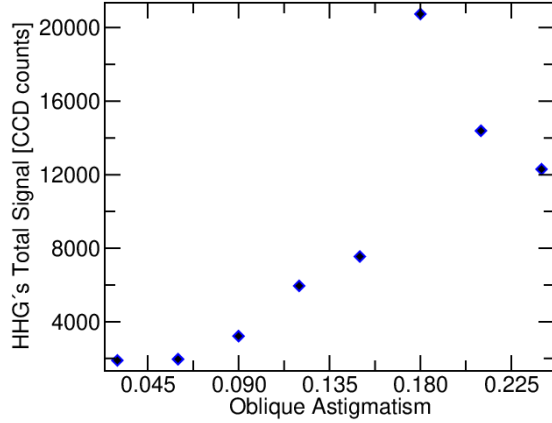
(a) Total HHG signal as a function of oblique astigmatism coefficient.
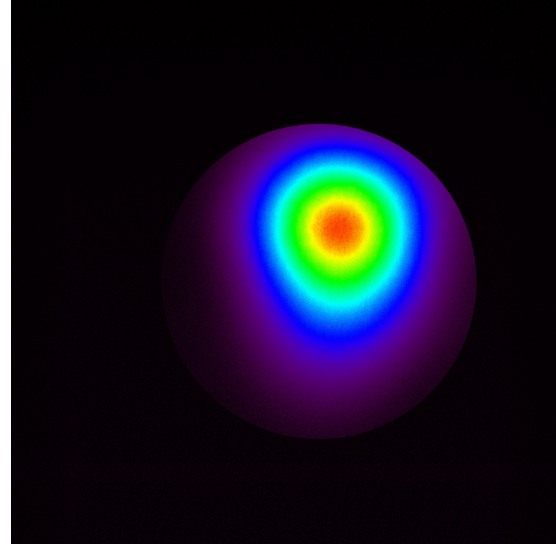
(b) Intensity map for oblique astigmatism coefficient of 0.18.

Figure 2: Manual optimisation results showing the effect of oblique astigmatism on HHG signal.

tion `foc_max_count` that returns the peak intensity detected in a camera image, and an optimisable variable `Zernikamplitudes_foc` with a specified search range (typically small values near zero, e.g., $[-0.6, -0.2]$) using MATLAB's `optimizableVariable` function. The `bayesopt` function then performs 30 iterations, exploring different values within the specified range to maximise `foc_max_count`. The optimal value is stored in `opt_focus`. This procedure is repeated for each of the four remaining aberration modes.

Subsequently, we refine the search ranges for each amplitude based on the individual optima (`opt_i`, where i = focus, coma1, etc.). We construct a new objective function `final_max_count` that returns the peak intensity using all five Zernike amplitudes simultaneously.

Finally, `bayesopt` performs 30 additional iterations to find the optimal combination of all five Zernike amplitudes within the refined search ranges.

5 Fourier Transform and Harmonics Wavelengths

5.1 New Camera

We adapted the script described in Section 4.2 to work with the Greateyes camera installed in the vacuum chamber. After analysing the available documentation and extensive testing, we successfully implemented the adaptation. This enabled a similar data acquisition process with improved image quality and resolution, and allowed analysis of data obtained directly from the vacuum chamber.

In this section, we analyse the frequencies and wavelengths of the harmonics generated in the laser system. After acquiring images with the ALEX-i camera (installed in the vacuum chamber) using the adapted script, we applied two algorithms: first, we computed the two-dimensional spatial Fourier transform of the input image; then, using

4

the Fourier transform as input, we used Python's `matplotlib` library to measure the distance between peaks in the transform. This analysis enables identification of the wavelengths present in the harmonic spectrum.

5.2 Applying the Fourier Transform

Using the ALEX-i camera, we acquired a large dataset of images from the harmonic system. A representative example is shown in Figure 3. Close inspection reveals at least two distinct frequencies in the harmonic signal, evident from the different spacings between the vertical interference fringes. For an interference pattern from multiple wavelengths, the fringe spacing is given by

$$w_i = z\frac{\lambda_i}{d},\qquad(1)$$

where $z \approx 3$ m is the distance between the source and the camera, and $d \approx 75\ \mu$m is the separation between the two HHG sources. Each wavelength λ_i produces fringes with spacing w_i. However, directly extracting these spacings from the raw image is difficult. We therefore apply a two-dimensional spatial Fourier transform, as shown in Figure 3.

The Fourier transform reveals peaks corresponding to spatial frequencies $k_i = 2\pi/w_i$. We measure the intensity of each peak within the region of interest (indicated by the red box in Figure 3) to determine the peak separations. To quantify k_i, we extract the intensity profile along a line that best captures the interference pattern in the two-dimensional Fourier transform, as shown in Figure 4.

From the intensity profile (Figure 4b), we can directly measure k_i values and determine the wavelengths present in the

harmonic spectrum. To calculate k_i, we identify peak pixel indices and use the ALEX-i camera specifications (pixel pitch of 13.5 μm) to convert to spatial frequency. Analysis of our dataset yielded the results shown in Table 1:

Analysis of Table 1 reveals inconsistent results. While the minimum fringe spacing $w_{\min} \approx 0.5$ mm matches expectations, the evolution of w_i and λ_i is not consistent across all cases. The fringe spacings and wavelengths do not follow the expected harmonic relationship. The algorithm successfully identifies $w_{\min}$ and $k_{\max}$, but signal noise and complexity make it difficult to reliably identify which peaks correspond to genuine harmonics, leading to inconsistent wavelength determination.

6 Neural Network

6.1 Motivation

Bayesian optimisation is a straightforward approach that optimises a single objective function (maximum pixel intensity). We initially attempted to incorporate roundness constraints by applying a modified Gaussian filter that preserves total intensity. However, this approach suffers from information loss, and improved filtered image quality does not necessarily indicate that the SLM is correcting the underlying aberrations. Only filters with $\sigma < 3$ were useful for noise reduction and suppression of sharp pixel intensities. We therefore explored deep neural networks as a more versatile and powerful solution.

We selected a Convolutional Neural Network (CNN) for this task. CNNs are powerful deep learning methods for image processing that recognise spatial patterns with translation invariance and
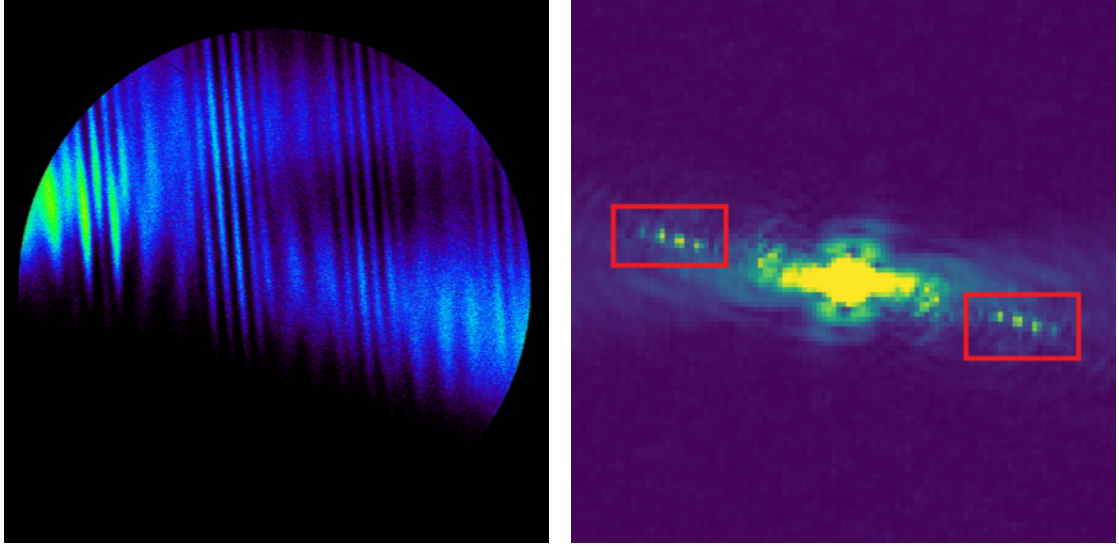
(a) Harmonic signal acquired with the ALEX-i camera.

(b) Two-dimensional spatial Fourier transform of the harmonic signal.

Figure 3: Harmonic signal and its Fourier transform.

Table 1: Fourier Transform Analysis.

Image	1			2				3			
Peak Pixel Index	166	184	202	182	187	190	195	168	175	180	186
k_i	13165	10416	7813	10706	9982	9548	8825	12731	11718	10995	10127
w_i [mm]	0.477	0.603	0.804	0.587	0.629	0.658	0.712	0.493	0.536	0.571	0.621
λ [nm]	11.93	15.08	20.10	14.68	15.73	16.45	17.8	12.33	13.4	14.28	15.53

extract meaningful features. Previous work has used CNNs to learn the mapping between object intensity distribution and aberration phase, with correction achieved by adding the conjugate of the wavefront aberration [4]. However, this approach requires either a Shack–Hartmann sensor for phase reconstruction or training on simulation data, which can lead to generalisation problems.

We instead use a CNN to learn the mapping between the point spread function (PSF) and Zernike coefficients. Correction is then achieved by applying the negative of the predicted coefficients to the SLM. This approach has been demonstrated previously [5], where Zernike polynomials of orders 4–15 (University of Arizona indexing scheme, shown in Figure 9) were used for correction.

6.2 Data Set Script

To generate training images, we introduce controlled aberrations by randomly generating Zernike polynomial coefficients of orders 4, 5, and 6 (University of Arizona indexing), which the SLM applies to modify the beam. We restrict our analysis to these orders for simplicity. We exclude piston, tip, and tilt (orders 1–3), as these do not represent true wavefront curvature aberrations.

A critical preprocessing step is selecting a single spot from the duplicated laser image and cropping appropriately. Our

6
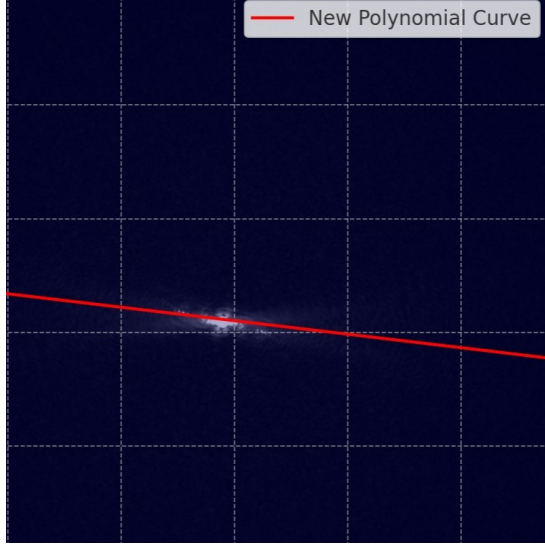
(a) Line extraction in Fourier space for peak analysis.
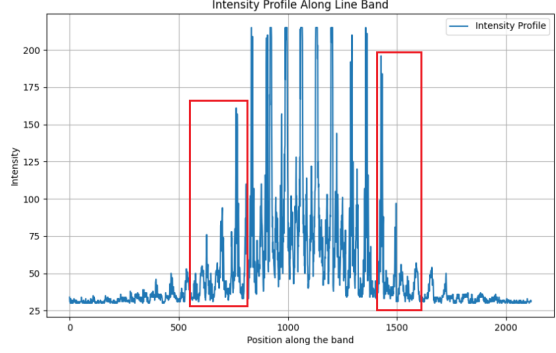
(b) Intensity profile along the extracted line showing distinct peaks.

Figure 4: Fourier space analysis for wavelength determination.

preprocessing script performs the following steps: (1) normalise the image to 8-bit range; (2) apply thresholding to create a binary image; (3) find contours in the thresholded image; (4) identify the largest contour by area; (5) crop the image to a standard bounding rectangle. Constant image size is required for the neural network input.

This preprocessing enables us to substantially increase the effective dataset size. Cases where the two spots are too close and both are captured are excluded from the dataset.

Using this procedure, we generated 506 image–coefficient pairs (PNG images and CSV files containing the corresponding Zernike coefficients) for our dataset. We note that our dataset is considerably smaller than those used in related work, which is a significant limitation. For example, Jin et al. [5] used 18,000 images of size 128×128 pixels. Our images were acquired from the HHG setup using a Thorlabs camera.

6.3 Neural Network Structure

The neural network architecture is crucial for the model's ability to extract and comprehend intrinsic patterns in the data. We designed a specific architecture for predicting Zernike coefficients from focal spot images. The network follows a sequential architecture incorporating convolutional, pooling, and dense layers. The detailed configuration is shown in Figure 6:

1) Convolutional and Pooling Layers:

- The first convolutional layer has 32 filters of size 3×3 with ReLU activation.

- A max-pooling layer (`MaxPooling2D`) with pool size 2×2 reduces dimensionality.

- The second convolutional layer has 64 filters of size 3×3 with ReLU activation.

Figure 5: Example of a preprocessed training image.

- A second max-pooling layer (2×2) is applied.

- The third convolutional layer has 64 filters of size 3×3 with ReLU activation.

2) Dense Layers:

- The convolutional output is flattened to a one-dimensional vector.

- A dense layer with 64 neurons and ReLU activation processes the flattened features.

3) Output Layer:

- The output layer has 3 neurons, corresponding to the three Zernike coefficients to be predicted.

- Linear activation is used, as this is a regression task.

This architecture is designed to capture spatial patterns in the images that correlate with Zernike coefficients, enabling accurate predictions through learned feature representations.

6.4 Hyperparameters and Training

Hyperparameters significantly influence model performance and generalisation. We used the following configuration:

6.4.1 Model Compilation

The model is compiled with the Adam optimizer, which is widely used for its effectiveness in training deep neural networks. The loss function is mean squared error (`mean_squared_error`), appropriate for regression tasks such as predicting Zernike coefficients. We monitor mean absolute error (`mae`) and accuracy (`accuracy`) as evaluation metrics during training.

6.4.2 Training Configuration

The dataset was split into training (70%), validation (15%), and test (15%) sets. Training was performed for 10 epochs with a batch size of 32. The learning rate was set to the default Adam value (10^{-3}). Early stopping was not employed, as the model showed consistent improvement throughout training.

6.5 Results

The training results, presented in Tables 2 and **??**, show the evolution of loss, mean absolute error (MAE), and accuracy metrics across training and validation epochs. The final test set evaluation is documented in Table **??**. Figure 7 visualises

Table 2: Training Results

Epoch	loss	mae	accuracy	val_loss	val_mae	val_accuracy
1	311.5240	3.6678	0.4431	0.2435	0.4036	0.5098
2	0.1999	0.3622	0.6559	0.1515	0.3165	0.8039
3	0.1369	0.2917	0.7426	0.1329	0.2934	0.7647
4	0.1061	0.2555	0.7995	0.0951	0.2453	0.7843
5	0.0663	0.2026	0.8119	0.0721	0.2039	0.8235
6	0.0468	0.1649	0.8441	0.0677	0.1995	0.7647
7	0.0307	0.1352	0.8564	0.0355	0.1449	0.8039
8	0.0219	0.1140	0.8911	0.0411	0.1450	0.8431
9	0.0155	0.0957	0.8985	0.0392	0.1440	0.8627
10	0.0137	0.0904	0.9233	0.0406	0.1391	0.8431

these results, showing promising performance.

The results demonstrate significant learning during training, with the model achieving 92.33% accuracy on the training set, 84.31% on the validation set, and 80.39% on the test set after 10 epochs. The test set performance provides insight into the model's generalisation to unseen data. The decreasing loss and MAE values, along with increasing accuracy, indicate successful learning of the mapping between focal spot images and Zernike coefficients.

7 Conclusion

We have presented a machine learning approach to optimise aberration correction in high-power laser systems for high harmonic generation. We implemented and compared two methods: Bayesian optimisation and a convolutional neural network.

Bayesian optimisation successfully optimised individual Zernike modes and their combinations, providing a baseline for comparison. However, this approach optimises only a single objective function (peak intensity) and requires sequential optimisation of each mode.

The CNN approach demonstrates promising results, achieving 80.39% accuracy on test data with a relatively small dataset of 506 images. The model successfully learns the mapping between focal spot images and Zernike coefficients, with consistent improvement over training epochs. The gap between training (92.33%) and test (80.39%) accuracy suggests some overfitting, which is expected given the limited dataset size.

The primary limitation of this work is the small dataset size compared to related studies. Expanding the dataset to thousands of images would likely improve generalisation and reduce overfitting. Future work should also explore: (1) incorporating additional Zernike modes beyond orders 4–6; (2) using the predicted coefficients in a closed-loop correction system; (3) comparing CNN performance directly with Bayesian optimisation on the same experimental setup; and (4) investigating transfer learning from simulation data to improve generalisation.

These results establish a foundation for automated aberration correction in HHG systems, with the potential to significantly improve beam quality and har-

monic generation efficiency.

8 Acknowledgements

References

[1] ZHONG, S. et al. **High harmonic generation in condensed matter**. Nature Reviews Physics, v. 4, p. 263-275, 2022.

[2] CORKUM, P. B. **Plasma perspective on strong field multiphoton ionization**. Physical Review Letters, v. 71, n. 13, p. 1994-1997, 1993.

[3] LAKSHMINARAYANAN, V.; FLEET, A. **Zernike polynomials: a guide**. Journal of Modern Optics, v. 58, n. 7, p. 545-561, 2011.

[4] WANG, K. et al. **Deep learning for wavefront sensing: a review**. Optics Communications, v. 487, 126823, 2021.

[5] JIN, K. et al. **Machine learning for adaptive optics**. Optics Express, v. 26, n. 21, p. 27869-27882, 2018.

A Appendix

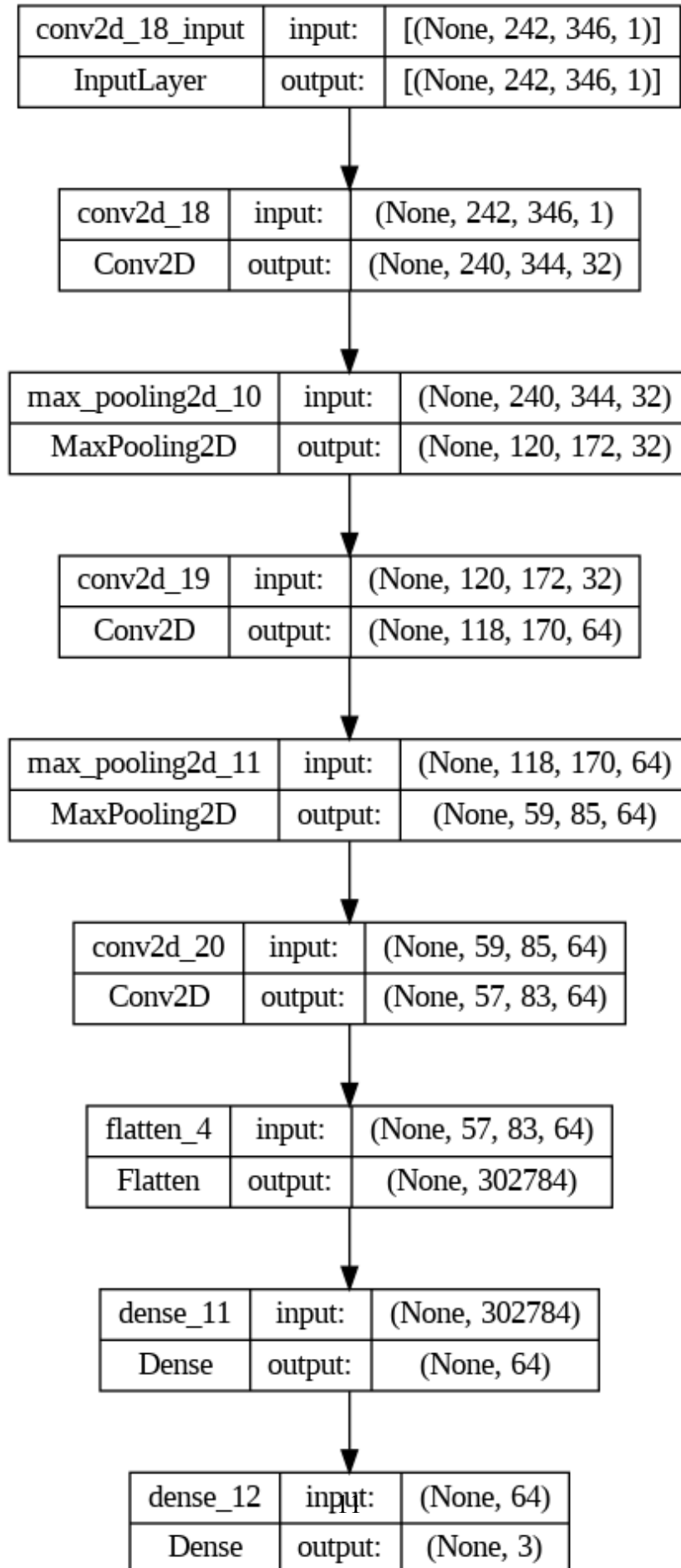Additional figures are provided below for reference.

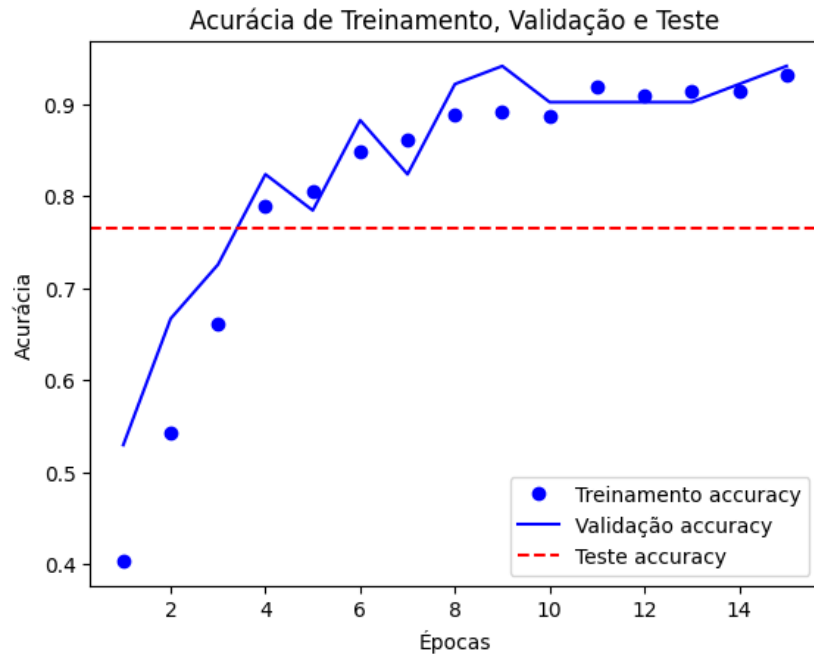Figure 6: Architecture of the convolutional neural network for Zernike coefficient prediction.

Figure 7: Training, validation, and test accuracy as a function of training epoch.
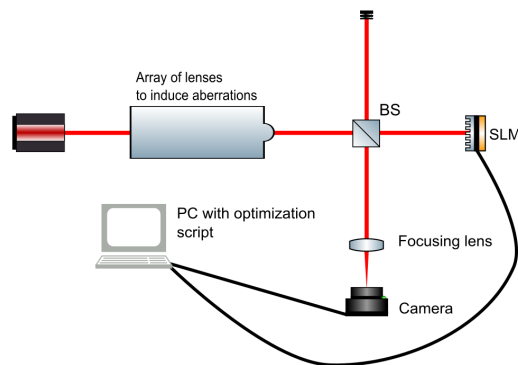

Figure 8: Initial setup for testing and developing optimization models.

Index	Zernike mode	Name
1	1	Piston
2	$2r \cos \theta$	Tip
3	$2r \sin \theta$	Tilt
4	$\sqrt{3}\,(2r^2 - 1)$	Defocus
5	$\sqrt{6}r^2 \cos 2\theta$	Astigmatism, 1st order
6	$\sqrt{6}r^2 \sin 2\theta$	Astigmatism, 1st order
7	$2\sqrt{2}(3r^3 - 2r) \cos \theta$	Coma
8	$2\sqrt{2}(3r^3 - 2r) \sin \theta$	Coma
9	$2\sqrt{2}r^3 \cos 3\theta$	Trefoil
10	$2\sqrt{2}r^3 \sin 3\theta$	Trefoil
11	$\sqrt{5}(6r^4 - 6r^2 + 1)$	Spherical aberration
12	$\sqrt{10}(4r^4 - 3r^2) \cos 2\theta$	Astigmatism, 2nd order
13	$\sqrt{10}(4r^4 - 3r^2) \sin 2\theta$	Astigmatism, 2nd order
14	$\sqrt{10}r^4 \cos 4\theta$	tetrafoil
15	$\sqrt{10}r^4 \sin 4\theta$	tetrafoil
...	...	...

Figure 9: Zernike Polynomials Scheme